PNAS
www.pnas.org

Supplementary Information for

A combined rheometry and imaging study of viscosity reduction in bacterial suspensions

Vincent A. Martinez, Eric Clément, Jochen Arlt, Carine Douarche, Angela Dawson, Jana Schwarz-Linek, Adama K. Creppy, Viktor Škultéty, Alexander N. Morozov, Harold Auradou, Wilson C. K. Poon

Vincent A. Martinez and Eric Clément.
E-mail: vincent.martinez@ed.ac.uk, eric.clement@upmc.fr

This PDF file includes:

www.pnas.org/cgi/doi/10.1073/pnas.1912690117

Supporting Information Text

Derivation of Eq.(4) of the main text

The theory outlined here is based on the mean-field treatment of microswimmer suspensions by Shelley and co-workers (1–3), and by Subramanian and Koch (4). We closely follow the method of Stenhammar et al. (5).

We consider a suspension of N microswimmers in a volume V at a finite number density $n = N/V$. The suspension is assumed to be dilute so that the only relevant interparticle interactions are defined by the far-field dipolar hydrodynamic fields generated by the microswimmers. The starting point of our theory is a mean-field, Smoluchowski-like equation

$$\frac{\partial}{\partial t}\Psi + \frac{\partial}{\partial x^\alpha}(\dot{x}^\alpha \Psi) + \mathbb{P}^{\alpha\beta}\frac{\partial}{\partial p^\beta}(\dot{p}^\alpha \Psi) = -\lambda\Psi + \frac{\lambda}{4\pi}\int d\boldsymbol{p}\ \Psi \quad [1]$$

for the one-particle distribution function $\Psi(\boldsymbol{x}, \boldsymbol{p}, t)$, which defines the probability of finding a microswimmer at the position $\boldsymbol{x}$ with the orientation given by a unit vector $\boldsymbol{p}$ at time t. The probability distribution function is assumed to be normalised

$$\int d\boldsymbol{x} d\boldsymbol{p}\ \Psi(\boldsymbol{x}, \boldsymbol{p}, t) = 1. \quad [2]$$

Within the mean-field description, each microswimmer obeys the following microscopic equations of motion

$$\dot{x}^\alpha = v_s p^\alpha + N\,\mathcal{U}^\alpha_{MF}, \quad [3]$$

$$\dot{p}^\alpha = N\,\mathbb{P}^{\alpha\beta}(\mathcal{W}^{\beta\gamma} + B\mathcal{E}^{\beta\gamma})p^\gamma, \quad [4]$$

where $\mathbb{P}^{\alpha\beta} = \delta^{\alpha\beta} - p^\alpha p^\beta$ is the projection operator, and $\delta^{\alpha\beta}$ is the Kronecker delta; Greek superscripts denote Cartesian components of vectors. The position of a microswimmer changes in time due to its self-propulsion with the swimming speed v_s and due to its advection by the velocity field $\boldsymbol{\mathcal{U}}_{MF}$, generated by the other swimmers

$$\mathcal{U}^\alpha_{MF}(\boldsymbol{x}, t) = \int d\boldsymbol{x}' d\boldsymbol{p}'\ u^\alpha_d(\boldsymbol{x} - \boldsymbol{x}', \boldsymbol{p}')\Psi(\boldsymbol{x}', \boldsymbol{p}', t), \quad [5]$$

where

$$u^\alpha_d(\boldsymbol{x}, \boldsymbol{p}) = \frac{\kappa}{8\pi}\frac{x^\alpha}{|\boldsymbol{x}|^3}\left[\frac{3(\boldsymbol{x}.\boldsymbol{p})^2}{|\boldsymbol{x}|^2} - 1\right]. \quad [6]$$

The velocity field $\mathbf{u}_d(\boldsymbol{x}, \boldsymbol{p})$ is generated at a position $\boldsymbol{x}$ by a force dipole located at the origin and oriented along the unit vector $\boldsymbol{p}$. The strength of the dipole is given by $\kappa = Fl/\mu$, where F is the magnitude of both dipolar forces, l is the dipolar length, and μ is the viscosity of the suspending fluid. Within the convention utilised here, $\kappa > 0$ corresponds to bacteria (pushers).

The orientation of a microswimmer changes due to two mechanisms. First is its passive rotation caused by the velocity gradients generated by the other microswimmers at its position. This mechanism is encoded in Eq. (4), where

$$\mathcal{W}^{\beta\gamma} = \frac{1}{2}\left(\frac{\partial}{\partial x^\gamma}\mathcal{U}^\beta_{MF} - \frac{\partial}{\partial x^\beta}\mathcal{U}^\gamma_{MF}\right), \quad [7]$$

$$\mathcal{E}^{\beta\gamma} = \frac{1}{2}\left(\frac{\partial}{\partial x^\gamma}\mathcal{U}^\beta_{MF} + \frac{\partial}{\partial x^\beta}\mathcal{U}^\gamma_{MF}\right), \quad [8]$$

are the vorticity and strain rate tensors. The parameter B in Eq. (4), related to the aspect ratio of a microswimmer, determines the type of orientational dynamics exhibited by a microswimmer: in an external shear flow, long and thin needles ($B = 1$) orient along the flow direction, while spheres ($B = 0$) rotate with a constant angular velocity. A bacterium is expected to interpolate between these limiting behaviours. The second mechanism is a random change in the microswimmer orientation (tumbling) with a rate λ, and is represented by the right-hand side of Eq. (1).

First we observe that Eq. (1) can be solved by setting the one-particle distribution function to a constant. The value of the constant is set by Eq. (2), yielding $\Psi(\boldsymbol{x}, \boldsymbol{p}, t) = 1/(4\pi V)$. This solution corresponds to a homogeneous and isotropic suspension. To assess its stability, we introduce a small perturbation around that state, $\Psi(\boldsymbol{x}, \boldsymbol{p}, t) = 1/(4\pi V) + \delta\Psi(\boldsymbol{x}, \boldsymbol{p}, t)$, and linearise Eq. (1) around the homogeneous and isotropic state, yielding the following equation of motion for the perturbation

$$\frac{\partial}{\partial t}\delta\Psi + v_s p^\alpha \frac{\partial}{\partial x^\alpha}\delta\Psi - 3B\frac{n}{4\pi}p^\alpha p^\beta \frac{\partial}{\partial x^\alpha}\delta\mathcal{U}^\beta + \lambda\ \delta\Psi - \frac{\lambda}{4\pi}\delta\rho = 0, \quad [9]$$

where we have introduced the velocity and density fluctuations

$$\delta\mathcal{U}^\alpha(\boldsymbol{x},\boldsymbol{p},t) = \int d\boldsymbol{x}'d\boldsymbol{p}'\ u_d^\alpha(\boldsymbol{x}-\boldsymbol{x}',\boldsymbol{p}')\delta\Psi(\boldsymbol{x}',\boldsymbol{p}',t), \tag{10}$$

$$\delta\rho(\boldsymbol{x},t) = \int d\boldsymbol{p}\ \delta\Psi(\boldsymbol{x},\boldsymbol{p},t), \tag{11}$$

and assumed that the fluid is incompressible. To reduce Eq. (9) to an algebraic form, we introduce the following ansatz

$$\delta f(\boldsymbol{x},\boldsymbol{p},t) = \frac{\mathrm{e}^{\chi t}}{(2\pi)^3}\int d\boldsymbol{k}\ \delta\hat{\Psi}(\boldsymbol{k},\boldsymbol{p})\mathrm{e}^{i\boldsymbol{k}.\boldsymbol{x}}, \tag{12}$$

where the sign of the real part of the temporal eigenvalue χ determines the linear stability of the homogeneous and isotropic base state. Upon substitution of Eq. (12) into Eq. (9), individual Fourier modes decouple, and we obtain

$$\begin{aligned}\chi\delta\hat{\Psi} + v_s ik^\alpha p^\alpha\delta\hat{\Psi} - 3B\frac{n}{4\pi}p^\alpha p^\beta ik^\alpha\delta\hat{\mathcal{U}}^\beta \\ + \lambda\delta\hat{\Psi} - \frac{\lambda}{4\pi}\delta\hat{\rho} = 0,\end{aligned} \tag{13}$$

where $\delta\hat{\rho}$ is the Fourier transform of the density fluctuations, while the velocity fluctuations are now given by

$$\delta\hat{\mathcal{U}}^\alpha(\boldsymbol{k}) = \int d\boldsymbol{p}\ \hat{u}_d^\alpha(\boldsymbol{k},\boldsymbol{p})\delta\hat{\Psi}(\boldsymbol{k},\boldsymbol{p}), \tag{14}$$

where $\hat{\boldsymbol{u}}_d$ is the Fourier transform of the dipolar field, Eq. (6),

$$\hat{u}_d^\alpha(\boldsymbol{k},\boldsymbol{p}) = -i\kappa\frac{(\boldsymbol{k}\cdot\boldsymbol{p})}{k^2}\left[\delta^{\alpha\beta} - \frac{k^\alpha k^\beta}{k^2}\right]p^\beta. \tag{15}$$

The density fluctuations $\delta\hat{\rho}$ decouple from the velocity fluctuations and do not lead to an instability (2, 5). We therefore drop them from Eq. (9) that can now be formally solved for $\delta\hat{\Psi}$. Substituting this solution into Eq. (14) gives

$$\delta\hat{\mathcal{U}}^\alpha = iB\frac{n}{4\pi}\delta\hat{\mathcal{U}}^\beta\int \mathrm{d}\boldsymbol{p}\ \frac{3p^\beta(\boldsymbol{p}\cdot\boldsymbol{k})\,u_d^\alpha(\boldsymbol{k},\boldsymbol{p})}{\lambda+\chi+iv_s(\boldsymbol{p}\cdot\boldsymbol{k})}. \tag{16}$$

Performing the integral yields the following equation for the temporal eigenvalue

$$\alpha = F(x), \tag{17}$$

where we have introduced

$$\alpha = \frac{v_s k}{3Bn\kappa}, \quad x = \frac{v_s k}{\lambda+\chi}, \tag{18}$$

and

$$F(x) = \frac{x\left(3+2x^2\right) - 3\left(x^2+1\right)\arctan(x)}{6x^4}. \tag{19}$$

To proceed, we observe that a good uniform approximation to $F(x)$ is given by

$$F(x) \approx \frac{1}{3\left(\frac{5}{x}+x+\frac{3}{2}\right)}, \tag{20}$$

which is obtained by combining the asymptotic behaviour of $F(x)$ as $x\to 0$ and $x\to\infty$. Using this approximation in Eq. (17), we finally obtain for the temporal eigenvalue

$$\chi = -\lambda + A(\alpha)Bn\kappa, \tag{21}$$

where

$$A(\alpha) = \frac{36\alpha^2}{2-9\alpha\pm\sqrt{-639\alpha^2-36\alpha+4}}. \tag{22}$$

In Fig. S1 we compare this approximation to $A(\alpha)$ extracted by solving the eigenvalue problem, Eq. (17), numerically. The agreement between the two approaches is semi-quantitative, and we, therefore, base our further analysis on Eq. (22).

As can be seen from Fig. S1 and Eq. (21), in an infinite system, the most unstable eigenvalue corresponds to $\alpha = 0$. Using the upper-branch value of $A(0) = 1/5$, we obtain the critical number density at the instability as

$$n_c^{\infty} = \frac{5\lambda}{B\kappa}, \qquad [23]$$

which has been derived previously (4, 5). To mimic the effects of confinement on the stability of the suspension, we limit the smallest available wavenumber to $k_{min} = 2\pi/H$, where H is the smallest dimension of the confining geometry. Solving

$$Re\left\{-\lambda + A\left(\frac{v_s k_{min}}{3Bn\kappa}\right) Bn\kappa\right\} = 0, \qquad [24]$$

yields the critical density in confinement

$$\frac{n_c(H)}{n_c^{\infty}} = 1 + \frac{3}{10}\frac{v_s k_{min}}{\lambda} + \frac{1}{5}\left(\frac{v_s k_{min}}{\lambda}\right)^2. \qquad [25]$$

This is Eq.(4) of the main text, where we switch from the critical number density ratio $n_c(H)/n_c^{\infty}$ to the critical volume fraction ratio $\phi_c(H)/\phi_c^{\infty}$, and use the average run-time $\tau = \lambda^{-1}$.

We want to stress that this approach gives only a qualitative estimate of the influence of confinement on the instability threshold as it does not impose the no-slip boundary conditions on the confining surfaces and ignores the wall-bacteria interactions discussed elsewhere (6–10).

Comparison of ϕ-dependency of low shear viscosity at three gap size

Figure 4a of the main text shows the ϕ-dependency of the effective viscosity measured at a shear rate of $\approx 0.04/s$ and a gap size $H = 500\mu m$. We show here in figure S2 results for other gap size and shear rates values in the low shear regime. While error bars of the viscosity values measured at the lowest shear rate $0.04/s$ and smallest gap size $H = 240\mu m$ are significantly large to draw any conclusion, all other datasets unambiguously discard the H^{-2}-dependency predicted by ALCT (11).

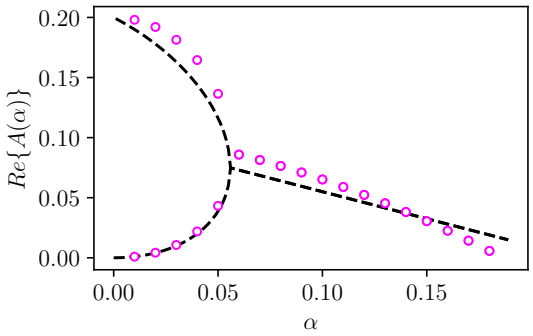

Fig. S1. $A(\alpha)$ vs α: Comparison between the numerical solution of $\mathrm{Eq.}\ (17)$ (circles) and the analytical approximation, $\mathrm{Eq.}\ (22)$, (dashed line).

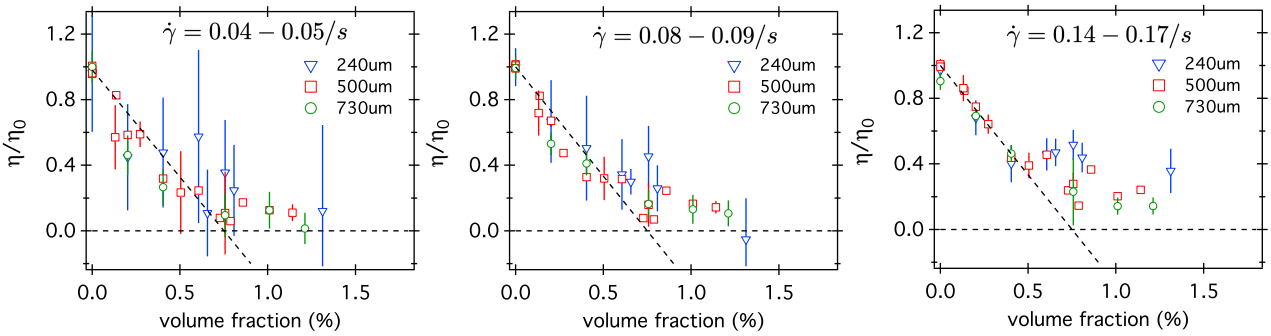

Fig. S2. The viscosity of $E.\ coli$ suspensions measured with three gap size $H = 240, 500, 730\,\mu\mathrm{m}$ at a shear rate $\dot{\gamma} \approx 0.04 s^{-1}$ (a), $\approx 0.08/s$ (b), and $\approx 0.15/s$ (c), as a function of volume fraction. The viscosity is normalised to the viscosity of the buffer $\eta_0(c_{\mathrm{serine}}) = (0.87 + 2.7 \times 10^{-4} c_{\mathrm{serine}})$ cP, with c_{serine} the concentration of serine used to prepare the solutions. Error bars are obtained from data analysis of individual measurements as in figure 3 of the main text. Dotted lines are guides to the eye.

References

1. Saintillan D, Shelley MJ (2008) Instabilities, pattern formation, and mixing in active suspensions. *Phys. Fluids* 20(12):123304.
2. Hohenegger C, Shelley MJ (2010) Stability of active suspensions. *Phys. Rev. E* 81:046311.
3. Saintillan D, Shelley MJ (2013) Active suspensions and their nonlinear models. *C. R. Physique* 14(6):497 – 517.
4. Subramanian G, Koch DL (2009) Critical bacterial concentration for the onset of collective swimming. *J. Fluid Mech.* 632:359–400.
5. Stenhammar J, Nardini C, Nash RW, Marenduzzo D, Morozov A (2017) Role of correlations in the collective behavior of microswimmer suspensions. *Phys. Rev. Lett.* 119(2):028005.
6. Berke AP, Turner L, Berg HC, Lauga E (2008) Hydrodynamic attraction of swimming microorganisms by surfaces. *Phys. Rev. Lett.* 101:038102.
7. Li G, Tang JX (2009) Accumulation of microswimmers near a surface mediated by collision and rotational brownian motion. *Phys. Rev. Lett.* 103:078101.
8. Elgeti J, Gompper G (2015) Run-and-tumble dynamics of self-propelled particles in confinement. *EPL* 109(5):58003.
9. Ezhilan B, Alonso-Matilla R, Saintillan D (2015) On the distribution and swim pressure of run-and-tumble particles in confinement. *J. Fluid Mech.* 781:R4.
10. Ezhilan B, Saintillan D (2015) Transport of a dilute active suspension in pressure-driven channel flow. *J. Fluid Mech.* 777:482-522.
11. Loisy A, Eggers J, Liverpool TB (2018) Active suspensions have nonmonotonic flow curves and multiple mechanical equilibria. *Phys. Rev. Lett.* 121(1):018001.